Question 1

A particle undergoing a 1-dimensional random walk has mean position equal to its original position:

$$< x_{random} > \; = x_0$$

Displacement due to drift: $v_d t$

$$x_{drift} = v_d t + x_{random}$$

No randomness associated with constant drift velocity, so $< v_d t > \; = v_d t$. Therefore:

$$< x>_{drift} = \; < v_d t + x_{random} > \; = \; = \; < v_d t > \; + \; < x_{random} >$$

$$< x>_{drift} = \; v_d t \; + \; x_0$$

The mean square displacement for just the random walk is given by:

$$< (x_{random} - x_0)^2 >= 2Dt$$

$$< x^2>_{drift} = \; < (v_d t)^2 > \; + \; 2 < v_d t(x_{random} - x_0) > \; + \; < (x_{random} - x_0)^2 >$$

$$< x^2>_{drift} = \; < (v_d t)^2 > \; + \; 2 < v_d t(x_0 - x_0) > \; + \; < (x_{random} - x_0)^2 >$$

$$< x^2>_{drift} = \; < (v_d t)^2 > \; + \; 0 \; + \; < (x_{random} - x_0)^2 > \; = (v_d t)^2 \; + \; < (x_{random} - x_0)^2 >$$

$$< x^2>_{drift} = \; (v_d t)^2 \; + \; 2Dt$$

Figure 1: Mean square displacement (μm^2) vs. time (s) at different velocities

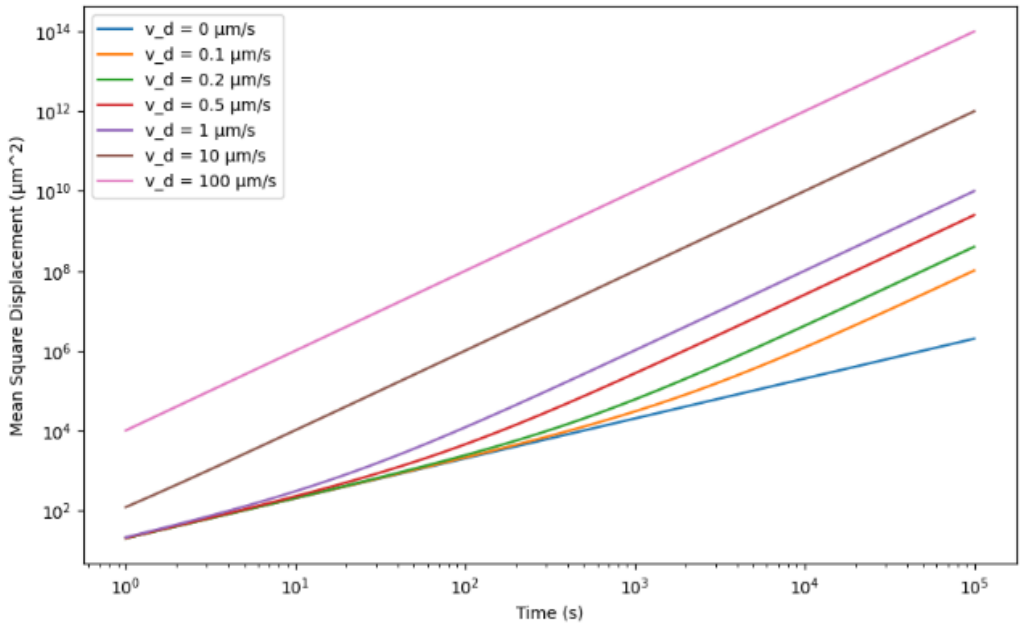

The slope with diffusion-dominated motion is around 1. The slope with velocity-dominated motion is around 2. With velocities that are in-between (ex. at 0.1μm/s), we note that the particle more closely embodies diffusion-dominated motion at lower times and velocity-dominated motion at higher times. This makes sense given that the t in the velocity term grows in a quadratic fashion, compared to the t in the random walk term.

Code screenshots

Generation of graph:

```python
import numpy as np
import matplotlib.pyplot as plt

D = 10 # we set our diffusion coefficient (µ^2 /s)

def mean_square_displacement(t, D, v_d):
    return 2 * D * t + (v_d * t) ** 2

time = np.logspace(0, 5, 100000) # we create time values from 1 to 100000

velocities = [0, 0.1, 0.2, 0.5, 1, 10, 100] # we generate multiple velocity values

plt.figure(figsize=(10,6))
for v in velocities:
    plt.loglog(time, mean_square_displacement(time, D, v), label=f"v_d = {v} µm/s")

plt.xlabel("Time (s)")
plt.ylabel("Mean Square Displacement (µm^2)")
plt.title("Mean Square Displacement vs. Time at different velocities")
plt.legend()
plt.show()
```

Generation of slope:

```python
v = 0 # variable velocity

# select two points on the line to calculate slope
id1 = 0
id2 = 100

t1 = time[id1]
t2 = time[id2]

log_msd1 = np.log(mean_square_displacement(t1, D, v))
log_msd2 = np.log(mean_square_displacement(t2, D, v))

log_t1 = np.log(t1)
log_t2 = np.log(t2)

slope = (log_msd2 - log_msd1) / (log_t2 - log_t1)
print(slope)
```

Question 2

Equation for mean-squared displacement with drift:

$$< x^2>_{drift} = (v_d t)^2 + 2Dt$$

Equation for mean-squared displacement without drift

$$< x^2 > = 2Dt$$

The true size of yeast cells obviously varies, but diploid cells are reported to have an ellipsoid shape with size 5×6 µm , and haploid cells 4 µm spheroids (Sherman, 2002). If we take the length of the cell to be 6 µm:

$$t = \frac{<x^2>}{2D}$$

$$t = \frac{(6\mu m)^2}{2(5\ \mu m^2/s)}$$

$$t = 3.6s$$

Rearranging for when mean-squared displacement includes a constant drift velocity:

$$< x^2>_{drift} = (v_d t)^2 + 2Dt$$

$$0 = (v_d t)^2 + 2Dt - < x^2>_{drift}$$

$$t = \frac{-2D \pm \sqrt{(2D)^2 - 4(v_d)^2(-(x^2)_{drift})}}{2(v_d)^2}$$

$$t = \frac{-2(5) \pm \sqrt{(2(5))^2 - 4(2)^2(-(6^2))}}{2(2)^2} = \frac{-10 \pm \sqrt{568}}{8}$$

$$t = 1.8s$$

The length of a moving fibroblast is reported to be $100\mu m$ (McDougall et al., 2006).

$$t_{no\ drift} = \frac{(100\mu m)^2}{2(5\ \mu m^2/s)} = 200.0s$$

$$t_{drift} = \frac{-2(5) \pm \sqrt{(2(5))^2 - 4(2)^2(-(100^2))}}{2(2)^2} = 48.8s$$

We can easily see that in the equation without drift velocity, the dependence on time is linear. Meanwhile, in the equation with drift velocity, the dependence on time is quadratic. Therefore, as the time term grows, the mean-squared displacement of the particle grows much more quickly if there is additional drift velocity.

The opposite relation is true: if the length is very large, then the time term for displacement with drift will be smaller compared to displacement without drift. The displacement term is linear in the time equation for displacement with drift, and quadratic in the time equation for displacement without drift. We can conclude that over long distances, it is not efficient to rely on just diffusion as a transport method.

References

McDougall, S., Dallon, J., Sherratt, J., & Maini, P. (2006). Fibroblast migration and collagen deposition during dermal wound healing: mathematical modelling and clinical implications. *Philos Trans A Math Phys Eng Sci*, *364*(1843), 1385-1405. doi.org/10.1098/rsta.2006.1773

Sherman, F. (2002). Getting started with yeast. *Methods in Enzymology*, *350*, 3-41. doi.org/10.1016/s0076-6879(02)50954-x

Question 3

We can rearrange for an equation for L_p

$$cos(\theta) = e^{-\frac{s}{2Lp}}$$
$$L_p = -\frac{s}{2ln(cos(\theta))}$$

I created a Python script to manually click on an image and add points along a filament. I modeled the filament using a spline function to interpolate between these points, allowing for a better curve representation. I approximated the curve's length by sampling 1,000 points and calculating the Euclidean distance between them. I then found the tangent lines at the endpoints by calculating the first derivative for the slope and used these to determine the angle between the lines. Screenshot attached at end.

I measured the scale bar, determining that one increment on either axis corresponds to 1000 nm. For accuracy, I took half the measurements from each image for both actin filaments and microtubules. Due to significant variation, I selected filaments with a single curve for measurement. For microtubules in the fibroblast, I chose those originating near the nucleus for clarity. In the myoblast, I focused on the outer lengths of microtubules to assess persistence length rather than individual tubulin filaments. For actin filaments, I selected areas near the top left nucleus of the myoblast image for reduced overlap with tubulin, and in the fibroblast, I opted for filaments with minimal overlap. Plots were generated with `matplotlib` and mean and standard deviation calculated with `numpy`.

Figure 2: Distribution of persistence lengths (µm) of 10 microtubules

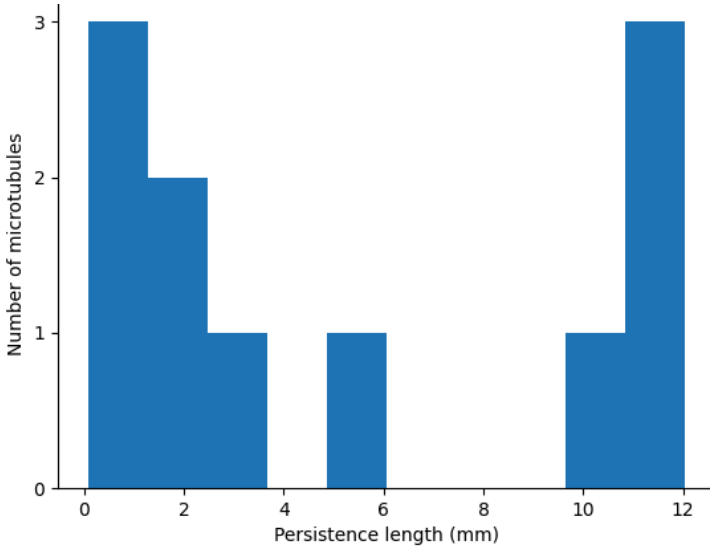

Figure 2: Distribution of persistence lengths (µm) of 10 actin filaments

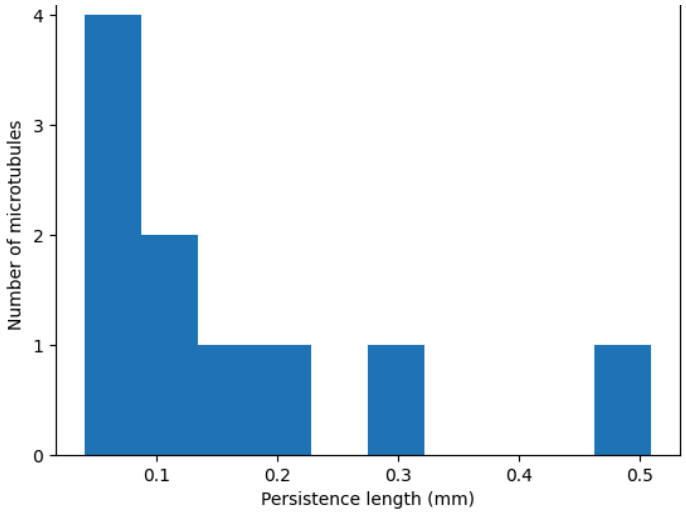

Table 1: Mean and standard deviation

	Microtubule	Actin
Mean (μm)	5300	160
Standard deviation	4700	100

Table

Source	Persistence length of microtubules (μm)	Persistence length of actin filaments (μm)
Own procedure	5400	160
Gittes, F., Mickey, B., Nettleton, J., & Howard, J. (1993).	5200	17.7
Wisanpitayakorn, P., Mickolajczyk, K. J., Hancock, W. O., Vidali, L., & Tüzel, E. (2022).	310 ± 90	9.9 ± 1.1
Niederriter, G., & Martin, D. S. (2019).	Microtubules of length <3 ranged from 0.15 to 4.5 Microtubules of length 15 and 4.5 ranged from 500 to 1800	N/A
Isambert, H., Venier, P., Maggs, A. C., Fattoum, A., Kassab, R., Pantaloni, D., & Carlier, M.-F. (1995).	N/A	Ranged from 9 - 20

The distribution of persistence lengths follows a bimodal shape. Since half of the measurements came from one image, and half from the other, it is clear that either the constitution or measurement of persistence lengths from one micrograph to the other was not consistent.

Measurement uncertainty was a major source of error. Across an extremely long filament (most lengths measurements were between 200 - 450 μm, it was difficult to obtain consistent degrees of curvature). This would have a drastic impact on the angles measured. Here, my persistence lengths are consistently greater than those found in literature, indicating that we are overestimating stiffness.

The resolution of the image was such that each filament was very small compared to the whole image. This could have resulted in certain angles being underestimated, since small curves could easily go under detected.

Niederriter et. al also note that persistence length varies across filaments of different length. Since the length was not standardized in the procedure, this would have caused greater variation.

Within these studies, microtubules and filaments were usually isolated from the cell and observed in another medium. However, inside the cell, there could be other forces impacting the bending of filaments. For example, in the crowded environment of the cytoplasm, protein attachment or linking with other nearby filaments can impact the mechanical properties of both actin and microtubule filaments.

References

Gittes, F., Mickey, B., Nettleton, J., & Howard, J. (1993). Flexural rigidity of microtubules and actin filaments measured from thermal fluctuations in shape. *Journal of Cell Biology*, *120*(4), 923-934. doi.org/10.1083/jcb.120.4.923

Isambert, H., Venier, P., Maggs, A. C., Fattoum, A., Kassab, R., Pantaloni, D., & Carlier, M. F. (1995). Flexibility of actin filaments derived from thermal fluctuations. *Journal of Biological Chemistry*, *270*(19), 11437–11444. https://doi.org/10.1074/jbc.270.19.11437

Niederriter, G., & Martin, D. S. (2019). Length-dependent persistence length for microtubules shorter than 3 micrometers. *Biophysical Journal*, *116*(3), 254a. https://doi.org/10.1016/j.bpj.2018.11.1387

Wisanpitayakorn, P., Mickolajczyk, K. J., Hancock, W., Vidali, O., & Tüzel, E. (2022). Measurement of the persistence length of cytoskeletal filaments using curvature distributions. *Biophysical Journal*, *121*(10), 1813-1822. https://doi.org/10.1016/j.bpj.2022.04.020

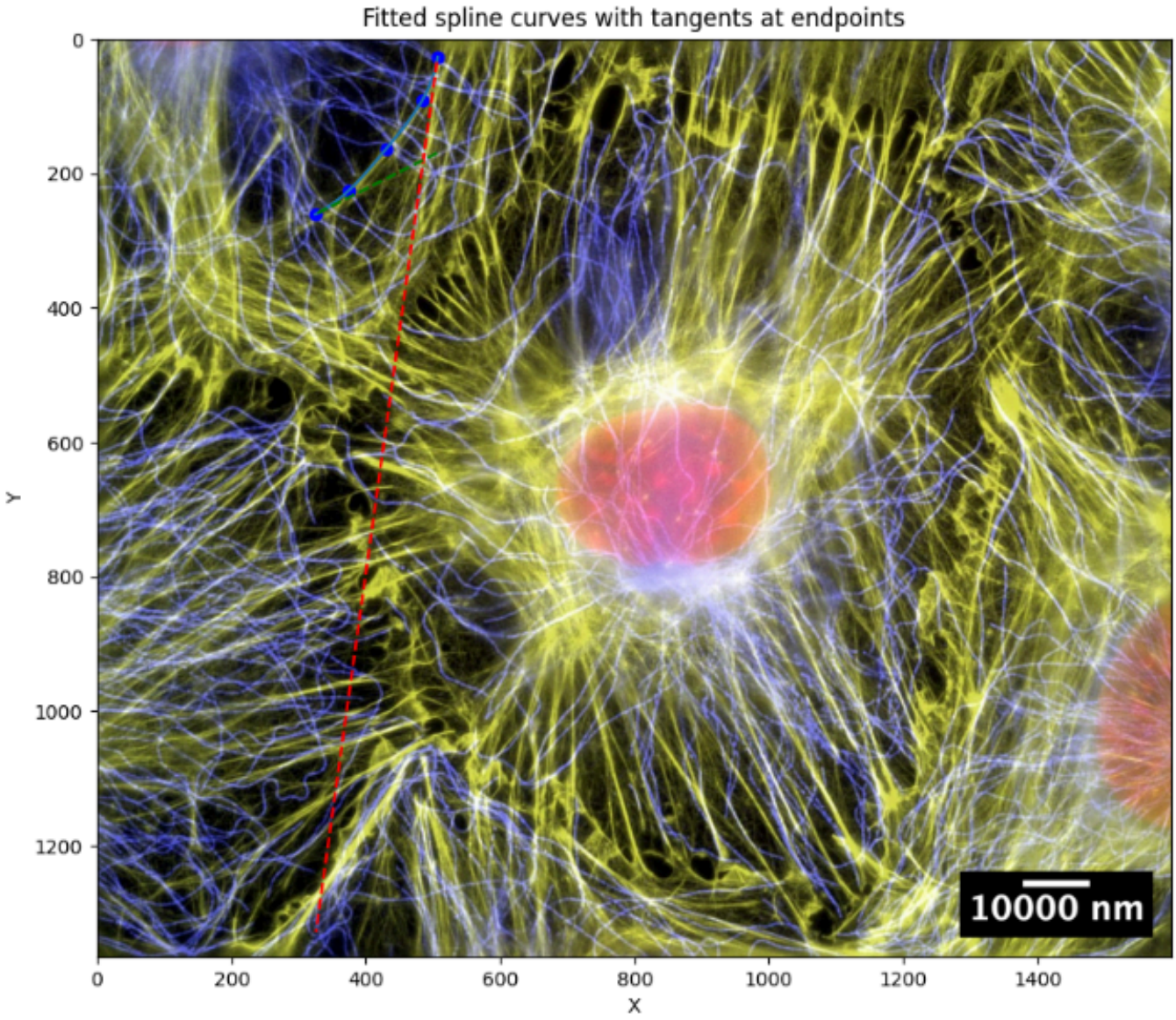
Fitted spline curves with tangents at endpoints
0
200
400
600
800
1000
1200
Y
0
200
400
600
800
1000
1200
1400
X
10000 nm

Question 4

a) In hard-boiled eggs, the presence of heat interferes with intermolecular interactions (such as hydrogen bonds or the single disulfide bridge) which stabilize the secondary and tertiary structure of the protein in raw eggs. Under low temperatures, within the egg white solution, the hydrophobic residues are folded towards the interior.

With denaturation, they become exposed towards the outside due to the disruption of bonds and interactions, and the increased hydrophobic interactions between adjacent unfolded ovalbumin molecules result in their aggregation. These molecules then engage in crosslinking of their beta-sheet structures, which results in the formation of a gel.

b) $\Delta G = \Delta H - T\Delta S$

When the egg is boiled, heat is added, which increases T and ΔH. The loss of protein folding results in an increase in disorder, so there is a positive ΔS. At high enough temperatures, $T\,\Delta\,S > \Delta H$ and there is a negative ΔG. This means that the ovalbumin in raw egg has higher free energy than in the hard-boiled egg.

c) Ovalbumin has only one disulfide bridge in a 385-amino acid chain length. Meanwhile, bovine pancreatic ribonuclease has 4 disulfide bridges in a 124-length amino acid chain. Disulfide bonds help stabilize the tertiary structure ("Disulfide Bonds in Protein Folding and Stability," 2018). It is likely that with more disulfide bridges, it is more energetically favourable to return to its native folded state, compared to with only a single disulfide bridge for a much larger molecule.

Figure 1: Visualization of the 4 disulfide bonds (in yellow) of bovine pancreatic ribonuclease

Figure 2: Visualization of the 1 disulfide bond (in cyan) of ovalbumin

In addition, at high temperatures, ovalbumin will form a gel due to the cross-linking of beta-sheets when the hydrophobic interior of the protein becomes exposed and multiple molecules begin to aggregate to reduce the total hydrophobic surface area (Mine, 1995). Energy is required to break these bonds and disrupt these interactions, and hence the process of refolding becomes energetically unfavourable, and the complex settles at a local free energy minima, even if the free energy of the folded protein is lower.

References

Disulfide Bonds in Protein Folding and Stability. (2018). In M. J. Feige (Ed.), *Oxidative Folding of Proteins: Basic Principles, Cellular Regulation and Engineering*. Royal Society of Chemistry. https://doi.org/10.1039/9781788013253-00001

Mine, Y. (1995). Recent advances in the understanding of egg white protein functionality. *Trends in Food Science & Technology*, *6*(7), 225-232. https://doi.org/10.1016/S0924-2244(00)89083-4